THE IMPACT OF CELL CROWDING AND ACTIVE CELL MOVEMENT ON VASCULAR TUMOUR GROWTH

Russell Betteridge

Centre for Mathematical Biology, Mathematical Institute,
University of Oxford, 24-29 St Giles', Oxford OX1 3LB, UK

Markus R. Owen, Helen M. Byrne

Centre for Mathematical Medicine, School of Mathematical Sciences
University of Nottingham, Nottingham NG7 2RD, UK

Tomás Alarcón

Bioinformatics Unit, Department of Computer Science
University College London, Gower Street, London WC1E 6BT, UK

Philip K. Maini

Centre for Mathematical Biology, Mathematical Institute
University of Oxford, 24-29 St Giles', Oxford OX1 3LB, UK

Abstract. A multiscale model for vascular tumour growth is presented which includes systems of ordinary differential equations for the cell cycle and regulation of apoptosis in individual cells, coupled to partial differential equations for the spatio-temporal dynamics of nutrient and key signalling chemicals. Furthermore, these subcellular and tissue layers are incorporated into a cellular automaton framework for cancerous and normal tissue with an embedded vascular network. The model is the extension of previous work and includes novel features such as cell movement and contact inhibition. We present a detailed simulation study of the effects of these additions on the invasive behaviour of tumour cells and the tumour's response to chemotherapy. In particular, we find that cell movement alone increases the rate of tumour growth and expansion, but that increasing the tumour cell carrying capacity leads to the formation of less invasive dense hypoxic tumours containing fewer tumour cells. However, when an increased carrying capacity is combined with significant tumour cell movement, the tumour grows and spreads more rapidly, accompanied by large spatio-temporal fluctuations in hypoxia, and hence in the number of quiescent cells. Since, in the model, hypoxic/quiescent cells produce VEGF which stimulates vascular adaptation, such fluctuations can dramatically affect drug delivery and the degree of success of chemotherapy.

1. **Introduction.** Cancer, together with cardiovascular disease, is the biggest killer in the Western World. The term cancer denotes hundreds of different diseases, each of which is characterised by deregulation of the homeostatic mechanisms that prevail in normal tissue. Thus, whereas normal cells are *social* entities whose behaviour and life cycle are intimately related to the function they perform and the tissue in which

---

they reside, cancer cells exhibit *selfish* behaviour, with uncontrolled proliferation and invasion routinely observed.

In spite of the massive resources devoted to cancer research, significant progress towards more efficient treatments is scarce. For many years, cancer research has been dominated by the so-called *gene-centric* approach, whereby the genetic mutations that occur in cancer cells are analysed. Attempts are then made either to reverse the mutations or to target the affected genes in order to eliminate cancer cells [18]. Although this approach is obviously sound and has produced a wealth of useful information on the different types of cancer, two serious problems threaten its viability as an effective therapeutic tool. Firstly, there is evidence that cancer genomes may be too unstable to be feasible therapeutic targets and too numerous to reverse (for example, 11000 genetic alterations per cell have been found in colorectal carcinoma). For further details, see the review by Folkman et al. [18] and references therein.

There is also strong evidence that epigenetic, cell-cell and intracellular interactions are instrumental in a tumour's development, so that tumour progression and growth are not simply products of genetic mutations. Tumour growth induces aberrant behaviour at all levels of tissue organisation, from gene expression to macroscopic tissue properties. These disturbances, in turn, feed back into the carcinogenic process, leading to the selection of more aggressive phenotypes that are better able to survive and progress in the increasingly abnormal environment. The ability of normal cells to survive in such tumour-modified environments becomes increasingly difficult. In this way, the cancer cells are able to out-compete their normal counterparts for space and resources. Two examples of this behaviour are the tumour-induced abnormalities in the vascular system and acidosis. We describe each phenomenon in turn below.

Tumour vessels frequently lack the well-defined anatomical structure of their normal counterparts, tortuous and leaky. Most of these effects are due to overexpression by the tumour of angiogenic factors, such as vascular endothelial growth factor. Endothelial cells of tumour blood vessels also exhibit abnormal profiles of protein synthesis and activity. Taken together these features result in highly irregular blood flow, which in turn leads to the appearance of extensive regions of hypoxia (i.e. low oxygen levels) [35]. Hypoxia is undesirable for two main reasons: it promotes drug resistance and favours the selection of more aggressive (e.g. invasive) phenotypes.

Tumour microenvironments are acidic due to the extensive use of glycolytic rather than aerobic metabolic pathways. Glycolytic metabolism is far less efficient than its aerobic counterpart and increases local pH levels. Whereas cancer cells are resistant to such acidic environments, normal cells struggle to survive in such conditions, thus losing their competitive advantage to the more resilient cancer cells. In fact, cancer cells are known to use glycolysis even in oxygen-rich conditions [24]. The information presented above illustrates the complexity of tumour growth and, in particular, the intricate way in which phenomena operating at different levels of biological organisation, i.e. on different time and length scales, may interact. Therefore, not only do we need to fully investigate processes occurring at a single scale (see, for example [6, 40, 50, 56] and references therein) but we must also determine emergent behaviour from their interactions (see, for example, [1, 3, 5, 10, 11, 25, 42, 48, 54]). In view of this, it seems that a full understanding of the dynamics of tumour growth requires that traditional (experimental) approaches be accompanied, and guided,

by theoretical approaches which can integrate the different physical phenomena. In an attempt to establish such an integrative modelling framework the authors have formulated a mathematical model, based on the hybrid cellular automaton concept [16, 48]. The framework accounts for blood flow and vascular adaptation, diffusion of nutrients, drugs and signalling cues, competition between normal and cancer cells, and intracellular processes such as cell division and apoptosis [3, 4, 13]. In the present paper, we extend our model to account for cellular crowding and cell movement. These two processes are of fundamental importance to study processes such as invasion [5], or new therapies based on tumour infiltration by engineered cells of the immune system, e.g. macrophages [12, 29, 47] or lymphocytes [45].

This paper is organised as follows. In Section 2, we summarise the general model framework and explain how cell crowding and cell movement are incorporated. In Section 3, we present our simulation results before considering, in Section 4, the effects of chemotherapy on the system. The paper concludes in Section 5 where we discuss our results and suggest possible directions for further research.
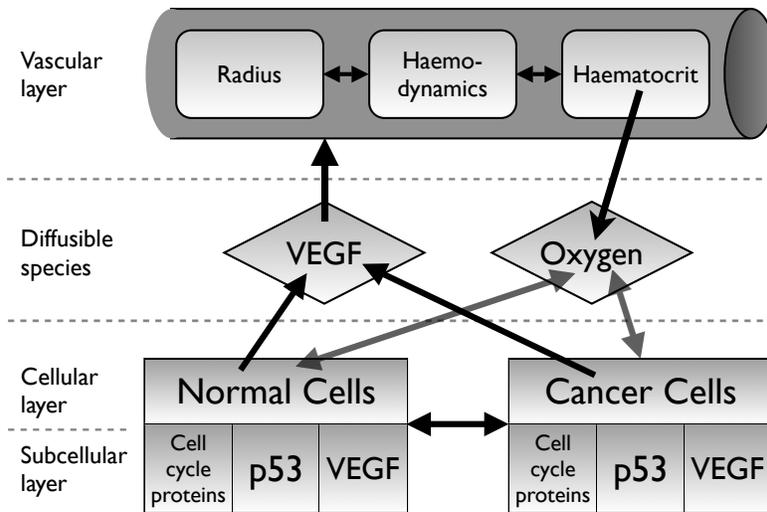

FIGURE 1. Basic structure of the model

2. **Model description.** In this section we summarise the main features of our multiscale model. The interested reader is referred to [3, 4, 13] for more detailed information, including parameter values.

2.1. **General model framework.** The model we use integrates phenomena occurring on very different time and length scales. These inter-related features include blood flow and structural adaptation of the vascular network, transport into the tissue of blood-borne oxygen, competition between cancer and normal cells, cell division, apoptosis and VEGF (growth factor) release. Our theoretical framework is based on the hybrid cellular automaton concept which has been used to model several aspects of tumour development (see [1, 5, 16, 48]). We extend this approach

to account not only for the presence of a diffusive substance (here oxygen) as in previous papers, but also to include intracellular and tissue-scale phenomena, and the coupling between them. To this end, we have organised our model into three layers: vascular, cellular, and subcellular, which correspond, respectively, to the tissue, cellular and subcellular time and length scales (see Fig. 1).

In the vascular layer, we focus on the structure of the network and blood flow (see [1] for more details). We consider a hexagonal vascular network (similar to that observed in liver) in which each individual vessel undergoes structural adaptation (i.e. changes in radius) in response to different stimuli. In addition to determining vessel radii we also compute the blood flow rate, the pressure drop and the haematocrit (i.e. relative volume of red blood cells) distribution in each vessel. Coupling between the vascular and cellular layers is mediated by the transport of blood-borne oxygen into the tissue. This process is modelled by a reaction-diffusion equation. The haematocrit acts as a distributed source of oxygen, whereas the cells act as spatially-distributed sinks of oxygen.

In the cellular layer, we focus on cell-cell interactions (competition) and the spatial distribution of the cells. We distinguish between normal and cancerous cells and assume that a given element may contain up to $N_{max} \geq 1$ cells (this extends earlier work in which $N_{max} = 1$). The two cell populations compete for space and resources, the cancerous phenotype usually performing better. Competition between the two cell types is introduced by simple rules, which connect the cellular and subcellular layers. Apoptosis (programmed cell death) is controlled by the expression of p53 (whose dynamics are dealt with in the subcellular layer): when the level of p53 in a cell exceeds some threshold the cell undergoes apoptosis. However, this threshold depends on the distribution of cells in a given neighbourhood.

Processes that are handled in the subcellular layer include cell division, apoptosis, and VEGF secretion, with ordinary differential equations (ODEs) being used to model the relevant biochemistry. One issue on which we focus is how the external conditions modulate the dynamics of these intracellular phenomena and, in particular, how the extracellular oxygen concentration affects the division rate, the expression of p53 (which regulates apoptosis) and the production of VEGF. Since the spatial distribution of oxygen depends on the spatial distribution of cells (cellular layer) and haematocrit (vascular layer), processes at the subcellular level are intimately linked to the behaviour of the other two layers: cell proliferation and apoptosis alter the spatial distribution of the cells (see Fig. 1); the cellular and the intracellular layers modulate the process of vascular structural adaptation through another transport process: diffusion of VEGF into the tissue and its absorption by the endothelial cells (ECs) lining the vessels.

2.2. **New model features.** As mentioned in the Introduction, the main aim of this paper is to extend our multiscale model to allow more than one cell to occupy an element in the cellular automaton and to account for cell movement. Additionally we introduce a more realistic method for calculating the haematocrit concentration. We describe these and other new features in turn below.

In order to account for cell crowding we introduce a carrying capacity $N_{max} \geq 1$; N_{max} denotes the maximum number of cells that can be located within an element of our cellular automaton. Additionally, we assume that vessels and cells may occupy the same locations, provided the constraints on carrying capacity are not violated. Further, while the size of each cell type is assumed to be equal, the carrying capacity of the vessels, tumour cells and normal cells may differ. In our

earlier work $N_{max} = 1$, and, since a particular element could contain at most one cell, successful division could only occur if there was an empty neighbouring site to which a daughter cell could move. Thus successful cell division was always accompanied by movement. Here, with $N_{max} \geq 1$, we treat cell proliferation and movement separately, first deciding whether a division can occur and then carrying out movement (note that division can only occur if a cell has successfully completed the cell cycle and this is determined at the subcellular level). If there is space for the daughter cell to remain in the same location as its mother then both will remain at that site. Otherwise, the daughter cell moves to the neighbouring cell with the largest oxygen concentration, assuming that this site has not reached its carrying capacity. This latter option means that for the case $N_{max} = 1$ cell division is treated identically to before, providing for a clean transition from previous implementations.

The rates of oxygen consumption and VEGF expression in the governing partial differential equations are adjusted to account for the number of cells (and their type) at each location.

Cell movement is modelled as a stochastic process, with transition probabilities depending on the numbers of cells in an element and adjacent elements. In more detail, the probability P_{ij} that a cell moves from site i to a neighbouring site j is assumed to be given by the number of vacancies at site j ($N_{max} - N_j$), divided by the total number of vacancies at site i and its neighbours plus an additional term, the inertia number M, which measures the tendency of cells stay at site i. For example, invasive cancer cells will have a lower inertia number than normal, non-invasive cells. Combining these ideas, we deduce that the transition probabilities P_{ij} have the following form:

$$
P_{ij} = \begin{cases}
\dfrac{N_{max} - N_j}{\displaystyle\sum_{k \in nbhd} (N_{max} - N_k) + N_{max}(1 + M) - N_i} & \text{for } i \neq j, \\[3em]
1 - \sum_k P_{ik} = \dfrac{N_{max}(1 + M) - N_i}{\displaystyle\sum_{k \in nbhd} (N_{max} - N_k) + N_{max}(1 + M) - N_i} & \text{for } i = j.
\end{cases}
$$

$$(1)$$

In the simulations, each active cell is given a chance to move, in an order which is randomised on each time step.

The movement rules described above resemble a reinforced random walk [46] due to the dependence on local and neighbouring cell numbers. We may consider the limit $N_{max} \to \infty$, for which we have a strictly unbiased random walk with

$$
P_{ij} = \frac{1}{K + 1 + M} \text{ for } i \neq j
$$

and

$$
P_{ii} = 1 - \sum_k P_{ik} = \frac{1 + M}{K + 1 + M}
$$

where $K = \sum_k 1$ measures the number of elements in the neighbourhood (unless otherwise stated, for the two-dimensional geometry considered here we have $K = 8$). The mean-waiting time for this random walk is $(K+1+M)/K$, which is proportional to the inertia number M.

In an improvement to the methods used in [1, 2, 3] and [4], we calculate vessel haematocrit according to Fung [19]. There are two cases to consider depending on

the structure of the vessel bifurcation. In case 1 the flow and haematocrit enters the bifurcation from the parent vessel (denoted f) and exits through two daughter vessels (denoted 1 and 2); for case 2 the flow enters from two vessels (again denoted 1 and 2) and exits through a single vessel (denote f). In both cases we assume that the flux of haematocrit is conserved across the bifurcation so that

$$\dot{Q}_f H_f = \dot{Q}_1 H_1 + \dot{Q}_2 H_2, \tag{2}$$

where $\dot{Q}_i$ and H_i denote the flux and haematocrit in vessel i.

For case 2 (two inflows, single outflow) we assume that the fluxes $\dot{Q}_1, \dot{Q}_2$ and $\dot{Q}_f$ and the incoming haematocrit concentrations are known and equation (2) is used to determine H_f. For case 1 (single inflow, two outflows) we assume that $\dot{Q}_f, \dot{Q}_1, \dot{Q}_2$ and H_f are known and that the following expression holds:

$$\frac{H_1}{H_2} - 1 = \alpha(H_f)\left(\frac{v_1}{v_2} - 1\right) = \alpha(H_f)\left(\frac{\dot{Q}_1 R_2^2}{\dot{Q}_2 R_1^2} - 1\right). \tag{3}$$

This equation describes a bias in the distribution of haematocrit due to differences in the daughter velocities v_1 and v_2 [19]. Given v_1 and v_2, we then solve equations (2) and (3) simultaneously to determine H_1 and H_2. In equation (3) $v_i = \dot{Q}_i/R_i^2$ denotes the velocity of vessel i and R_i denotes its radius. The dependence of α on H_f is supported by experimental data presented by Fung [19] showing that, for case 1, as the haematocrit in the parent vessel increases the bias in H_1 and H_2 due to differences in daughter velocities decreases. For example, as H_f approaches one, the haematocrit must split almost symmetrically, with $H_1 \approx H_2 \approx H_f \approx 1$. For these reasons and for simplicity, henceforth we fix $\alpha(H_f) = (1 - H_f)$.

Broadly speaking, our model works as follows. The vessel network adapts its structure in response to mechanical and metabolic cues, setting up a pattern of haematocrit which serves as a distributed source for oxygen in a partial differential equation to describe oxygen diffusion. We assume that cells serve as point sinks of oxygen. The cells themselves are progressing through the cell cycle in a manner determined by a set of coupled nonlinear ordinary differential equations describing the temporal dynamics of key proteins in the cell cycle. Cells divide accordingly or, under hypoxic conditions, undergo quiescence, apoptosis or begin to produce VEGF, which modifies the vasculature allowing more nutrient to infiltrate the region. The full details of the model may be found in the series of papers [1, 2, 3].

3. **Simulations.** We consider as initial condition the set-up in Figure 2, namely the introduction of a small number of tumour cells into a region of vascularised normal tissue. We explore the effects of the novel features that have been added to the original model, namely the phenomena of cell movement and over-crowding (contact-inhibition).

Before we describe the results below, we briefly review the consequences of the improved haematocrit splitting. Previous implementations have used $H_f = H_1 + H_2$ rather than equation (2), so that haematocrit is diluted at branches where a parent flows into two daughters, or concentrated at branches where two parents flow into a single daughter. Consequently, in such a case oxygen and haematocrit concentrations peak close to the inflow and outflow (see Figure 3 and [4, 13]). This should be compared with the new distributions in Figure 2. In particular, in the new, more realistic formulation the haematocrit concentration is maximal along the path of maximal flow from inlet to outlet.
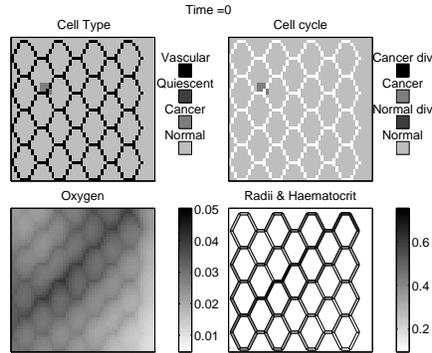
FIGURE 2. Initial conditions for all simulations. At $t = 0$ a small number of tumour cells are introduced into the vascularised tissue. At this time, the vasculature and oxygen concentration are at their quasi-steady states, with haematocrit flowing predominantly down the path of least resistance.
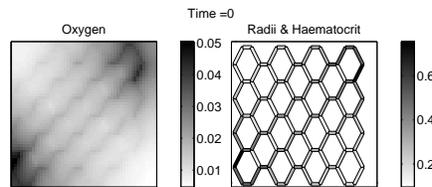

FIGURE 3. Oxygen distribution and vascular structure for previous implementations of haematocrit-splitting using $H_f = H_1 + H_2$ [3, 4, 13] rather than equation (2). Haematocrit concentration is diluted/concentrated at branches, so haematocrit and oxygen levels are maximal close to the inflow (bottom left) and outflow (top right).

3.1. **Impact of cell movement on tumour growth.** Figure 4 shows results from a basic model simulation where the normal and tumour cells move only as a result of cell division (i.e. $M \to \infty$ in equation (1) and $N_{max} = 1$, so that cells can only divide by placing daughter cells in a vacant neighbouring site). In consequence, tumour invasion requires the creation of empty spaces. In this model normal cells develop lower p53 thresholds for apoptosis when their neighbourhood comprises predominantly tumour cells, and therefore die, creating the necessary space for tumour cell invasion. As the tumour spreads, hypoxia leads to the formation of quiescent regions which stimulate vessel enlargement and more uniform haematocrit, and consequently oxygen, distributions. Figure 4 also illustrates which normal and tumour cells are dividing. At any given time this number is relatively small, and concentrated predominantly in well-oxygenated areas.

In Figure 5 we present results showing how including active cell movement (with $M = 50$) influences the tumour's development. Comparing Figures 4 and 5 we see that tumour cell movement leads to significantly more rapid invasion. More cell movement also means that cells can migrate into the corners of the tissue domain (which are particularly low in oxygen). Tumour cells in such regions ultimately
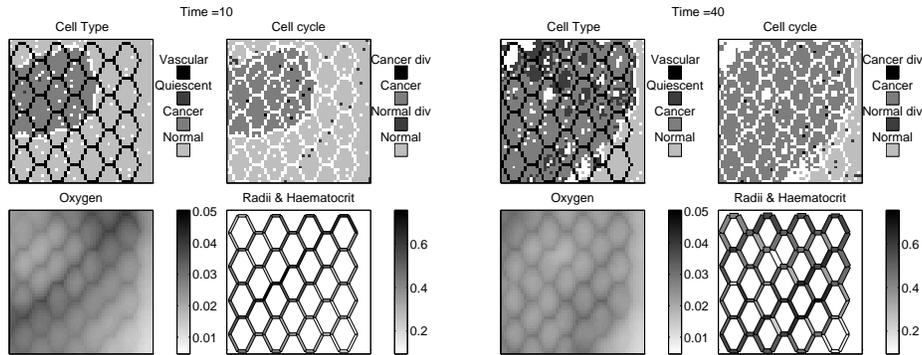
FIGURE 4. Output from a basic simulation (no active cell movement and carrying capacity of one) at times $t = 10$ (left) and $t = 40$ (right). The cell cycle panel indicates that at any given time there are relatively few dividing cells. As the tumour spreads, hypoxia leads to the appearance of quiescent cells which stimulate vessel enlargement and a more uniform haematocrit, and consequently oxygen, distributions. Parameter values: $M \to \infty$ and $N_{max} = 1$.

die, but before this happens normal cells also located in the corners die (via competition/changing normal cell thresholds) so that at large times very few normal cells remain in the tissue. This is also reflected in a widening of the sparsely populated margin between the tumour mass and surrounding normal tissue as the inertia number M decreases (this is particularly apparent for $M = 5$, results not shown).
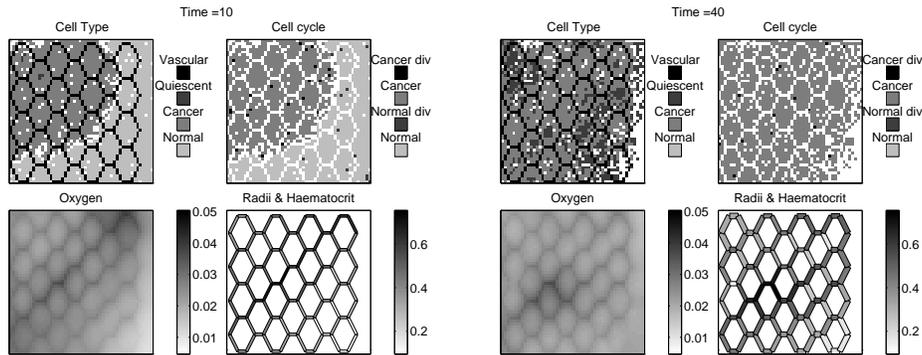

FIGURE 5. Output at times $t = 10$ (left) and $t = 40$ (right) from a simulation with active movement for comparison with Figure 4. We note that when movement is included, tumour cell infiltration is more rapid and there are greater fluctuations in the number of quiescent tumour cells. Parameter values: $M = 50$ and $N_{max} = 1$.

Figure 6 summarises how tumour growth changes as the inertia number M varies. Decreasing M gives more rapid and complete colonisation of the domain, and larger fluctuations in quiescent cell numbers. We also see how the average vessel radius follows these fluctuations, this phenomenon being mediated by the production of VEGF by the quiescent cells.
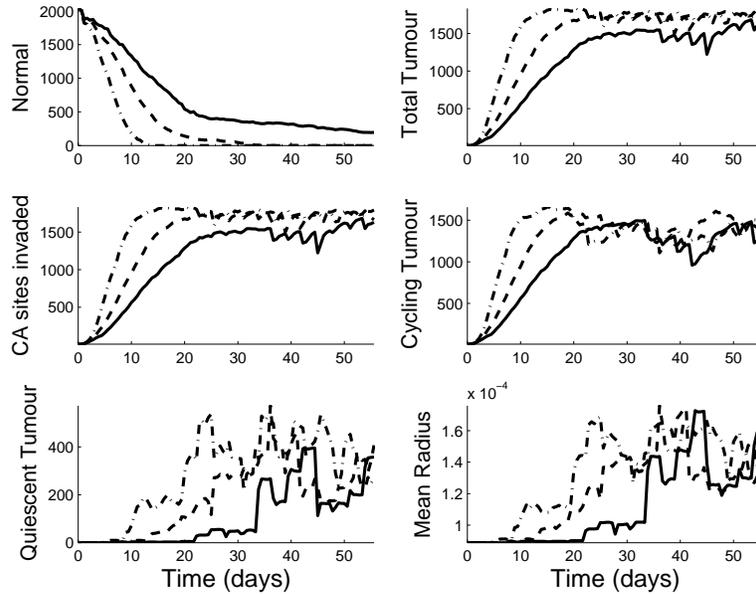
FIGURE 6. Summary data showing how, when $N_{max} = 1$, changes in the inertia number M influence the evolution of the number of normal cells, the total number of tumour cells, the number of CA locations occupied by one or more tumour cell, the number of non-quiescent tumour cells, the number of quiescent tumour cells, and the mean vessel radius. In general the number of CA locations occupied by one or more tumour cells gives a measure of the extent of tumour invasion. Since for this simulation $N_{max} = 1$ the number of CA location occupied by one of more tumour cells is identical to the total tumour cell number. Key: Solid line, no movement ($M \rightarrow \infty$); dashed line, $M = 50$; dot-dashed line, $M = 5$.

3.2. **Impact of over-crowding on tumour development.** In this section we assume that cells only divide locally (unless they have reached carrying capacity), and there is no other source of cell movement. The tumour will thus expand only when it has locally reached carrying capacity, and hence our simulations show a dense tumour that invades more slowly than one with a lower carrying capacity (see Figure 7 and compare with Figure 4). A tumour of this type would therefore be more manageable than a population with active movement. As the summary data presented in Figure 8 shows, as the carrying capacity N_{max} increases there is a trade-off between increased cell number and high cell density. Indeed, as N_{max} increases the total number of tumour cells decreases due to increases in hypoxia and the attendant cell death. This also leads to much larger fluctuations in quiescent tumour cell numbers and the mean vessel radius. Altering this balance would probably require a reduction in the rate at which tumour cells consume oxygen, the reduction being in line with the increase in local cell density.

Indeed, Figure 9 shows how reducing the rate of oxygen consumption per cell by a factor equal to the carrying capacity significantly increases the tumour cell population, although the initial rate of tumour invasion does not match that with
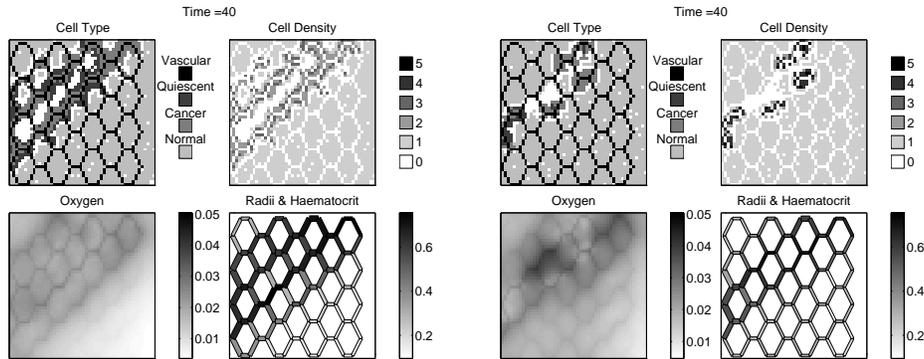
FIGURE 7. Results from a pair of simulations showing how increasing the tumour cells' carrying capacity (N_{max}) changes the tumour's size and structure at time $t = 40$. As N_{max} increases invasion is substantially reduced (compare also with Figure 4). Parameter values: $N_{max} = 3$ (left hand plots); $N_{max} = 5$ (right hand plots).
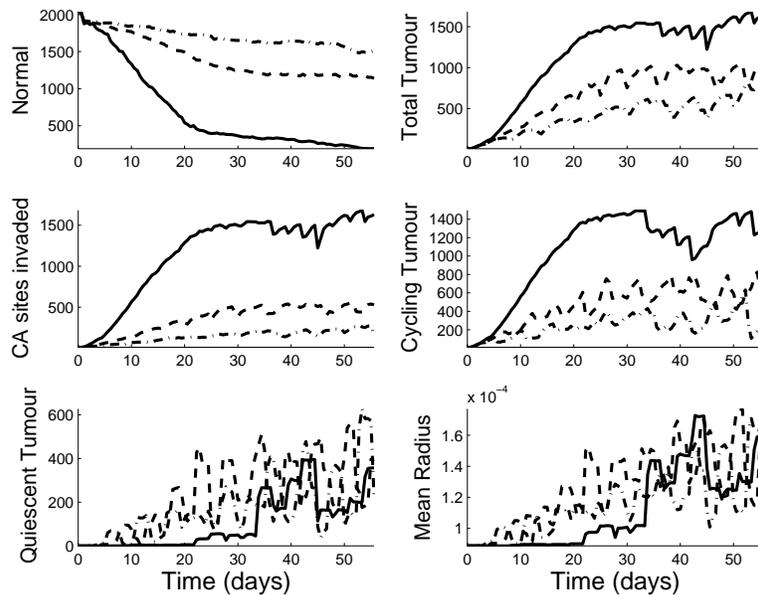

FIGURE 8. Summary data for the simulations presented in Figures 4 and 7 showing how the tumour's size and composition change as the tumour cell carrying capacity N_{max} varies. As N_{max} increases the total number of tumour cells and their colonisation of the tissue decrease. This is because local increases in cell number lead to hypoxia and cell death, without a compensatory increase in invasiveness. Key: solid line, $N_{max} = 1$; dashed line, $N_{max} = 3$; dot-dashed line, $N_{max} = 5$.

$N_{max} = 1$. Another consequence of having a lower rate of oxygen consumption is that there is a considerable reduction in the number of quiescent cells.
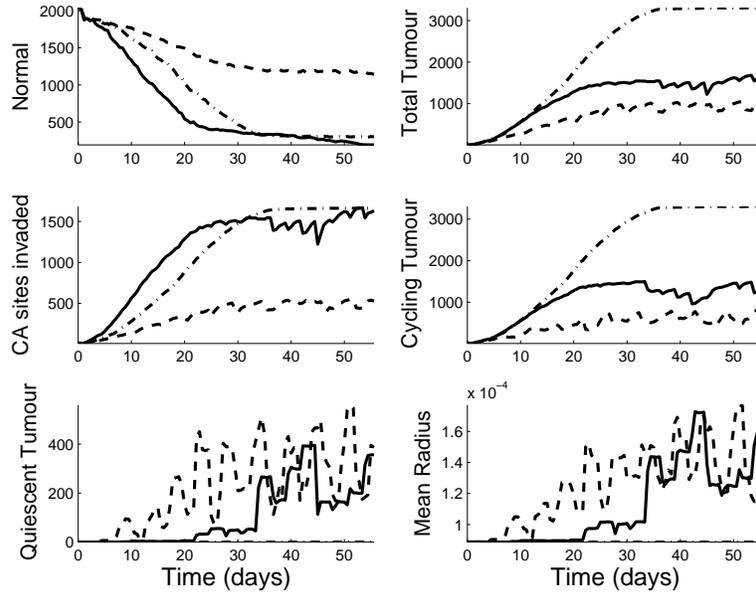

FIGURE 9. Summary data showing how varying the tumour cells' carrying capacity (N_{max}) and their rate of oxygen consumption affects the system's dynamics. We observe that increasing N_{max} and decreasing the rate of oxygen consumption significantly increases the number of tumour cells but not invasion. Key: solid line, $N_{max} = 1$, with standard rate of oxygen consumption; dashed line, $N_{max} = 3$ with standard rate of oxygen consumption; dot-dashed line, $N_{max} = 3$, with rate of oxygen consumption by tumour cells reduced by factor of $N_{max} = 3$.

3.3. **Combined effects of active movement and over-crowding.** In this case there is a complex balance between enhanced invasion due to cell movement and reduced invasion associated with higher local densities: increasing the carrying capacity has different effects depending on the rate of tumour cell movement. As we have already seen, when tumour cells cannot move, except via cell division, increasing their carrying capacity reduces the rate of invasion and the overall rate of growth of the tumour cell population (see Figure 8). Even when tumour cells can move actively, increasing the carrying capacity **still** decreases the rate of tumour invasion, although the growth in the total number of tumour cells is not necessarily retarded. This is accompanied once more by large fluctuations in quiescent cell numbers and the mean vessel radius (Figure 10).

Figure 11 illustrates how, for a fixed value of the tumour carrying capacity, increasing the rate of movement increases the speed of invasion and the tumour's overall growth. Combining these results, we see that increases in carrying capacity must be accompanied by increases in motility in order to maintain invasiveness, in the absence of other factors such as reductions in nutrient consumption.
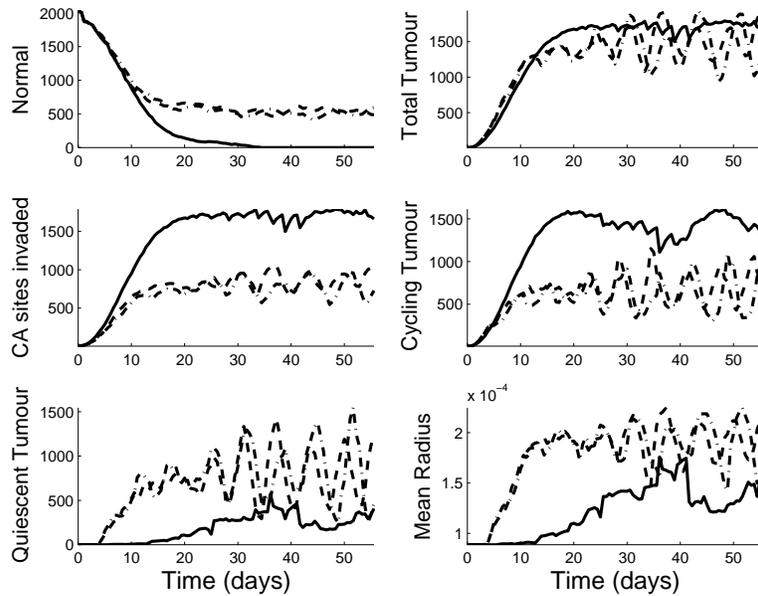
FIGURE 10. Summary data showing how changes in the tumour cell carrying capacity (N_{max}) affect the system dynamics when there is active tumour cell movement ($M = 50$). Even with substantial tumour cell movement, increasing N_{max} gives a decrease in invasion speed. Although the invasion speed is reduced, the total number of tumour cells grows more rapidly and to greater numbers than without cell movement (compare Figure 8). Key: solid line, $N_{max} = 1$; dashed line, $N_{max} = 3$, dot-dashed line, $N_{max} = 5$.

4. **The impact of chemotherapy.** We now investigate how active movement and over-crowding affect the dynamics when a blood-borne antiproliferative drug is introduced into the system. We assume that the drug is continuously administered to the vessels and, hence, that the drug concentration at the inlet vessel is held constant. Furthermore, as in [4], we assume that the drug is carried in the plasma, and hence that its concentration in a particular vessel is proportional to $1 - H$, where H is the haematocrit concentration in that vessel. We treat the vessels as distributed sources of drug and assume that, once the drug leaves the vessels, it diffuses through the tissue and is taken up by the normal and healthy cells.

Denoting by θ and θ_{vess} the drug concentrations in the tissue and vessels respectively, we solve the following diffusion equation, with no-flux boundary conditions, to determine the drug concentration in the tissue at a given time:

$$0 = D_\theta \nabla^2 \theta + h_\theta(\theta_{vess} - \theta) - \lambda_{drug}\theta. \tag{4}$$

In Eq. (4), D_θ denotes the assumed constant diffusion coefficient of the drug, h_θ the rate at which it is transported across the vessel wall and λ_{drug} the assumed constant rate at which the drug decays. Importantly, $\theta_{vess} = \theta_{adm}(1 - H)$ where θ_{adm} is the administered drug dose. We further assume that the drug works in the following manner. When a cell attempts to divide, if the drug concentration exceeds a threshold value θ_{kill} then the cell fails to divide and is itself killed.
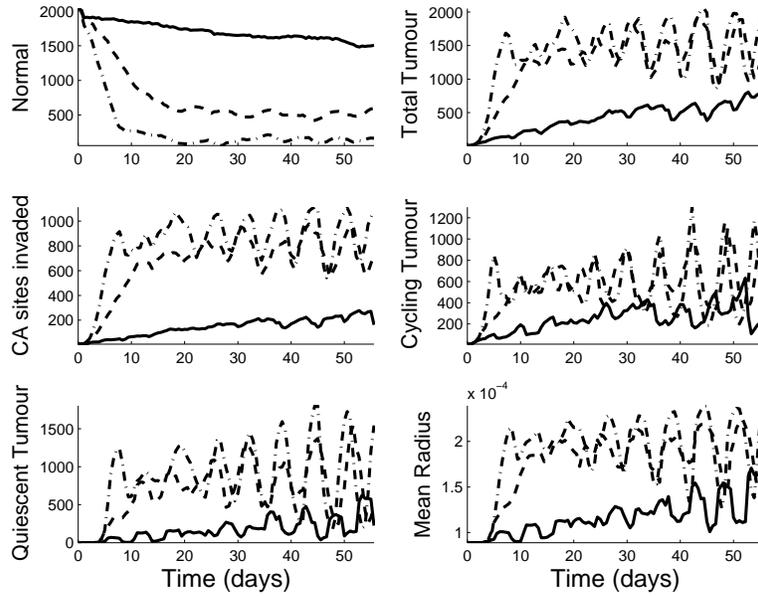
FIGURE 11. Summary data showing how, for a fixed tumour cell carrying capacity ($N_{max} = 5$), changes in the degree of tumour cell movement (M) affect the system dynamics. With $N_{max} = 5$, as the inertia number increases the rates at which the tumour invades and increases in cell number also increase, this effect being more pronounced for larger values of N_{max} (compare Figure 6). Key: solid line, no movement ($M \to \infty$); dashed line, $M = 50$, dot-dashed line, $M = 5$.
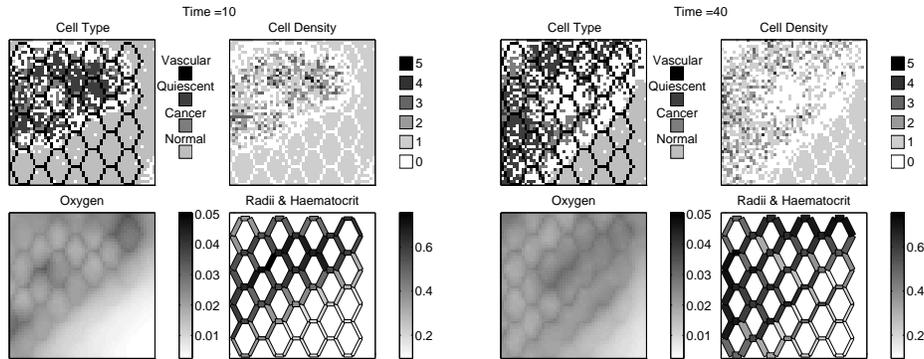

FIGURE 12. Output at times $t = 10$ (left) and $t = 40$ (right) from a simulation with active cell movement ($M = 50$) and cell crowding ($N_{max} = 5$). Invasion is substantially enhanced in comparison to Figure 7 (where $N_{max} = 5$ and $M \to \infty$), but not in comparison to Figure 5 (where $N_{max} = 1$ and $M = 50$).

For θ_{adm} sufficiently large, all regions of simulated tissue will have $\theta > \theta_{kill}$, and such a simulated treatment would be guaranteed to eradicate a tumour (but also all normal cells). On the other hand, for θ_{adm} small enough, no regions will experience high enough drug levels to induce cell kill. We are interested here in the marginal case for which drug levels are close to θ_{kill}, such that inhomogeneities in blood flow and cell distributions may or may not give rise to significant cell kill. As a base example, Figure 13 shows the effect of a marginal dose of drug on normal tissue. Since H is inhomogeneous, and tends to be greatest down the diagonal, in the absence of tumour-induced stimuli such as VEGF, the drug concentration will tend to be maximal away from the diagonal (top left and bottom right). Thus, if the drug concentration is close to the threshold required for cell death upon division, this inhomogeneity will result in some regions being above threshold, and others below. Thus we see in Figure 13 that normal cells are only killed in relatively small numbers. We now wish to explore how changes in haematocrit distribution due to the presence of a tumour alter the drug distribution and the consequent effects of the drug on a growing tumour.
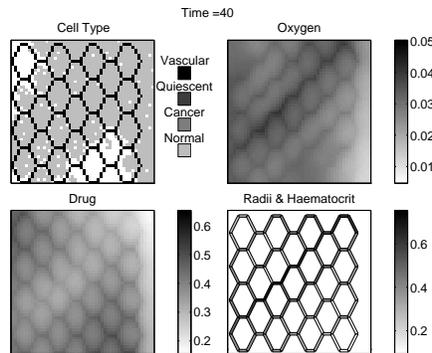

FIGURE 13. Output at time $t = 40$ Drug delivery to normal tissue. Since drug delivery is proportional to $1-H$, its distribution is complementary to that of oxygen. Normal cells are killed at the top left and bottom right of the tissue region, where drug concentrations are maximal. Drug is administered according to equation (4), with $D_\theta = 0.00145, h_\theta = 8, \lambda_{drug} = 2$, and $\theta_{vess} = \theta_{adm}(1 - H)$ with $\theta_{adm} = 4.625$.

Figure 14 shows how movement alone affects drug treatment in this marginal situation. There is only a small effect on the growth of the tumour, since the magnitude of fluctuations in haematocrit is insufficient to create large regions with $\theta > \theta_{kill}$.

Figure 15 shows how movement affects drug treatment when the tumour cell carrying capacity is larger (in this case $N_{max} = 5$). There is a much greater effect on tumour growth due to increased numbers of VEGF-producing quiescent cells, which in turn cause inhomogeneity in haematocrit and drug delivery. The effect is particularly strong when a larger carrying capacity is combined with significant tumour cell movement.

5. **Discussion.** Given that biological function does not arise as a property of any one spatial scale, to investigate fully biological phenomena multiscale approaches
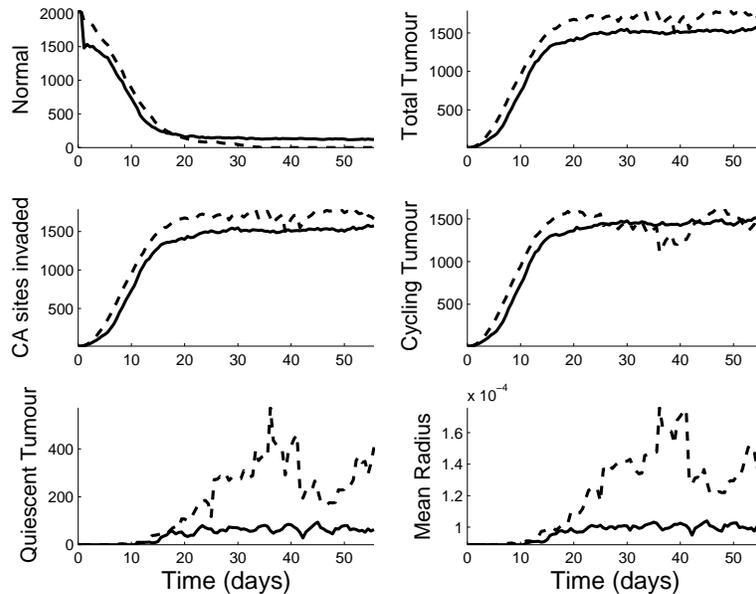
FIGURE 14. Summary data showing the response to chemotherapy of a tumour for which $N_{max} = 1$ and $M = 50$. We note that in this case the drug has little effect on the total number of tumour cells but does reduce significantly the number of quiescent cells and the fluctuations in both their number and the mean vessel radius. Key: solid line, with drug; dashed line, without drug. Parameter values for drug delivery: as in Figure 13.

need to be adopted. In this paper, we have extended our preliminary multiscale models for vascular tumour growth to incorporate cell movement, over-crowding, and more realistic dynamics for haematocrit distribution. We have investigated the resultant effects of these and shown they can greatly affect tumour cell invasion dynamics. We also investigated, briefly, the effects of drug treatment.

Our model is for a "generic" tumour in that it includes generic processes. To apply our model to a real situation we need to focus on a particular cancer. Future work, therefore, will include specialising the model to describe specific tumours.

We are presently working on implementing the general model framework in a modular way that will allow easy expansion. Processes that are currently described phenomenologically will be easily replaced by "slot-in" mechanistic models as more data becomes available. For example, in the present model we include the effects of glycolytic metabolism of tumour cells on normal cells by lowering the apoptotic threshold for normal cells (to reflect the fact that the acidic by-products of glycolysis are toxic to normal cells). This is a very important process and we will need to include more detailed models of this, together with the somatic evolution that is proposed to arise as a consequence [24, 59].

Many multiscale models to date include, at best, very weak coupling and feed-backs between levels and this is biologically unrealistic. For example, one might expect that the inertia number, M, in our model should be a function of oxygen
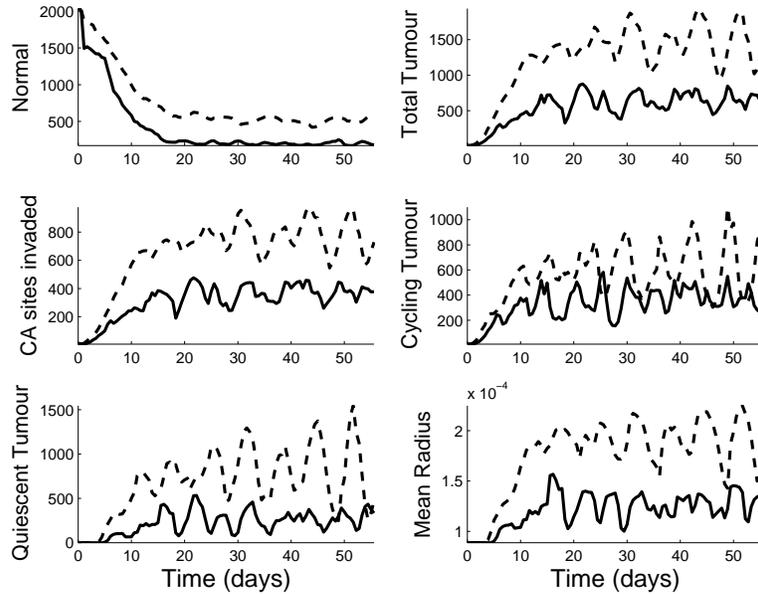
FIGURE 15. Summary data showing the response to chemotherapy of a tumour for which $N_{max} = 5$ and $M = 50$. Comparison with Figure 14 ($N_{max} = 1$) shows how a larger value of N_{max} leads to more extensive hypoxia. The resulting increase in VEGF levels creates inhomogeneities in blood flow and drug concentration, leading to a much stronger chemotherapeutic effect. Key: dashed line, no drug; solid line, with drug.
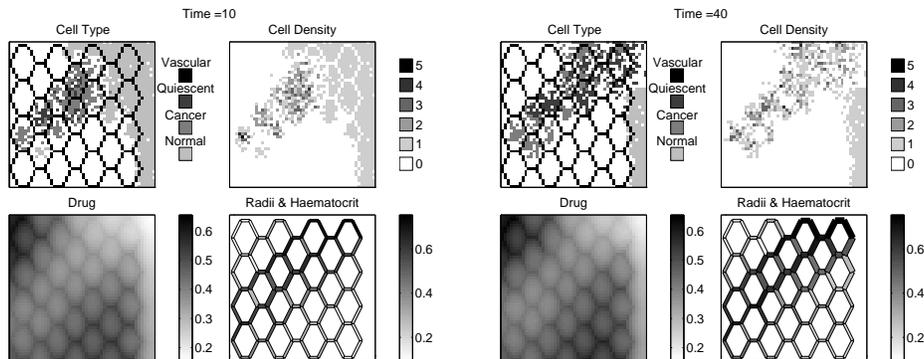

FIGURE 16. Output at times $t = 10$ (left) and $t = 40$ (right) from a simulation in which a tumour with $N_{max} = 5$ and $M = 50$ is exposed at a blood-borne drug. Comparison with Figure 12 shows that the drug has a significant effect on the tumour's growth.

concentration, becoming infinite at low oxygen levels (no oxygen means that cells cannot move) and decreasing as the oxygen concentration increases.

At the vascular level, we could make the model more realistic by including a number of features. For example, greater flexibility is needed concerning the number

and location of inlet and outlet vessels. Given the highly tortuous and irregular nature of tumour vasculature, it is also important to relax our assumption that the vasculature lies on a hexagonal lattice and to consider instead arbitrary geometries. This modification is also needed to account explicitly for the new branches that are formed during angiogenesis. Recent work by Gevertz and Torquato illustrates how some of these changes may be accomplished [25]. Finally, introducing a carrying capacity for the cells and vessels, so that more than one cell may occupy a given site, means that the number of cells surrounding vessels may vary markedly in time and space. This information could be used to estimate the mechanical force being exerted on the vessels by the cells and hence to allow for phenomena such as occlusion of vessels by rapidly proliferating tumour cells, such features being common in immature tumour vessels [30].

Another noteworthy feature of [25] is their use of Voronoi tessellations rather than cellular automata to model the cells. Other alternatives that exist and whose relative strengths and weaknesses should be assessed include Potts models [63] and agent-based models [60].

With a more realistic model of the tumour vasculature, it should be possible to study the role of endothelial progenitor cells (EPCs) and, in particular, the relative contribution of vasculogenesis and angiogenesis to the formation of new tumour vessels. This balance may provide insight into why existing anti-vascular therapies often fail and aid the development of more effective anti-vascular therapies.

Our preliminary results suggest that the impact of chemotherapy is strongly related to the behaviour of the tumour and the ways in which the vasculature and haematocrit concentration are modelled. For example, a mutant population characterised by the ability to move through the tissue will be less sensitive to chemotherapy than a population which has an elevated carrying capacity (compare Figures 14 and 15). These results highlight the difficulties associated with designing therapies that can successfully target the different subpopulations within a tumour without causing excessive damage to healthy tissue. In particular our results suggest that a drug of the type studied here would have limited success when used to treat glioblastoma, a highly invasive brain tumour with poor patient prognosis [64, 65, 66]. Biopsies from glioblastomas suggest that the tumours typically contain cells of two main phenotypes: some cells are highly proliferative with low motility (i.e. high carrying capacity and high inertia number) while others are highly motile with low proliferation rates (i.e. low inertia number and carrying capacity). By extending our model to distinguish between such phenotypes and then exposing the tissue to chemotherapy, we expect that the highly motile cancer cells would be largely insensitive to the drug while the less motile cells would be preferentially targeted. Additionally, if we wish to use the model to investigate the effects of particular therapies, then we need also to construct and analyse models that account in more detail for the manner in which the drugs actually work [17, 31, 32, 53].

Cells of the immune system, such as lymphocytes and macrophages, are increasingly the target for novel genetic therapeutic interventions [12, 29, 45], and there has been considerable work modelling such tumour–immune system interactions (see [8, 47] and references therein). Such immune cells are noted for their ability to migrate through tissues, including densely-packed tumours, and this migration is an important factor in many immunotherapies — genetically modified immune cells are typically delivered in the blood, and must leave the bloodstream and migrate through tissues before acting on tumour cells. Thus it is essential to include cell

movement in our multiscale model framework, in order to explore the dynamics of tumour–immune system interactions. In future work we will introduce immune cells, such as macrophages, via the vasculature, allowing them to extravasate (i.e. leave the vasculature) at a rate that depends on stimuli such as VEGF. In order to allow such cells to migrate through tissue containing normal and tumour cells, we must allow variable carrying capacities at each automata location, as outlined in this paper. Modifications to the transitions rates defined in equation (1) will allow the inclusion of leukocyte chemotaxis, a key mechanism whereby white blood cells can target, for example, hypoxic tumour regions.

The extensions mentioned above will certainly make the model more realistic biologically but we run the risk of rendering it, at the same time, clinically useless because of computational tractability and expense. Perhaps one of the great challenges that applied mathematics faces this century is to be able to reduce multiscale models in biology to make them tractable. At the moment the mathematics required to do this does not exist.

REFERENCES

[1] T. Alarcón, H.M. Byrne, P.K. Maini. *A cellular automaton model for tumour growth in a heterogeneous environment.* J. theor. Biol. (2003) **225**, 257–274.

[2] T. Alarcón, H.M. Byrne and P.K. Maini. *A mathematical model of the effects of hypoxia on the cell-cycle of normal and cancer cells* J. Theor. Biol. **229** (2004), 395–411.

[3] T. Alarcón, H.M. Byrne, P.K. Maini. *A multiple scale model of tumour growth.* Multiscale Model. Simul. (2005) **3**, 440–475.

[4] T. Alarcón, M.R. Owen, H.M. Byrne, P.K. Maini. *Multiscale modelling of tumour growth and therapy: the influence of vessel normalisation on chemotherapy.* Computational Mathematical Methods in Medicine. (2006). To appear.

[5] A.R.A. Anderson. *A hybrid mathematical model of solid tumour invasion: the importance of cell adhesion.* Math. Med. Biol. **22** (2005), 163-186.

[6] R.P. Araujo and D.L.S. McElwain . *A history of the study of solid tumor growth: the contribution of mathematical modelling.* Bull. Math. Biol. **66**(2004), 1039-1091.

[7] K. Bartha and H. Rieger. *Vascular network remodelling via vessel co-option, regression and growth in tumours.* Preprint. Available from the arXiv/Q-Bio repository: http://arxiv.org/abs/q-bio.TO/0506039. (2006).

[8] N. Bellomo and E. de Angelis. *Strategies of applied mathematics towards an immuno mathematical theory on tumors immune system interactions.* Math. Models Meth. Appl. Sci. **8:**(1998), 1403–1429.

[9] N. Bellomo, E. de Angelis and L. Preziosi . *Multiscale modelling and mathematical problems related to tumor evolution and medical therapy.* J. Theor. Med. **5**(2003), 111–136.

[10] N. Bellomo and P.K. Maini *Preface.* Math. Mod. Meth. Appl. **15**(11) (2005), iii-viii.

[11] N. Bellomo and P.K. Maini *Preface.* Math. Mod. Meth. Appl. **16**(S1) (2006), iii-vii.

[12] B. Burke, S. Sumner, N. Maitland, and C.E. Lewis, *Macrophages in gene therapy: cellular delivery vehicles and in vivo targets*, J. Leuk. Biol., **72** (2002), 417-428.

[13] H.M. Byrne, M.R. Owen, T. Alarcón, J. Murphy, P.K. Maini. *Modelling the resopnse of vascular tumours to chemotherapy: a multiscale approach.* Math. Model. Meth. Appl. Sci. (2006) **16**(S1), 1–25.

[14] V. Cristini, J. Lowengrub and Q. Nie. *Nonlinear simulation of tumour growth.* J. Math. Biol. **46**(2003), 191-224.

[15] E. De Angelis and L. Preziosi . *Advection-diffusion models for solid tumour evolution in vivo and related free boundary problems*, Math. Models Methods App. Sci., **10**(2000), 379-407.

[16] A. Deutsch, S. Dormann. *Modeling of avascular tumor growth with a hybrid cellular automaton.* In Silico Biol. **2** (2002), 1–14.

[17] H. Enderling, A.R. Anderson, M.A. Chaplain, A.J. Munro and J.S. Vaidya. *Mathematical modelling of radiotherapy strategies for early breast cancer*. J. theor. Biol. **241** (2006), 158-171.

[18] J. Folkman, P. Hahnfeldt, L. Hlatky. *Cancer: looking outside the genome*. Nature Rev. Mol. Cell Biol. **1** (2000), 76–79.

[19] Y.C. Fung. "Biomechanics: Circulation", Second Edition, Springer Verlag, New York.

[20] A. Gamba, D. Ambrosi, A. Coniglio, A. de Candia, S. Di Talia, E. Giraudo, G. Serini, L. Preziosi and F. Bussolino . *Percolation, morphogenesis, and burgers dynamics in blood vessel formation*. Phys. Rev. Lett., **90**(2003), 118101.

[21] L.B. Gardner, Q. Li, M.S. Parks, W.M. Flanagan, G.L. Semenza and C.V. Dang. *Hypoxia inhibits* G_1/S *transition through regulation of p27 expression*. J. Biol. Chem. **276** (2001), 7919–7926.

[22] R.A. Gatenby and E.T. Gawlinski.*The glycolytic phenotype in carcinogenesis and tumor invasion: insights through mathematical models*. Cancer Res. **63** (2003), 3847–3854.

[23] R.A. Gatenby and P.K. Maini. *Mathematical Oncology*. Nature. **421** (2004), 321.

[24] R.A. Gatenby and R.J. Gillies. *Why do cancers have high aerobic glycolisis?*. Nature Reviews Cancer **4** (2004), 891-899.

[25] J.L. Gevertz and S. Torquato. *Modelling the effects of vasculature evolution on early brain tumour growth*. J. theor. Biol. (2006) [Epub ahead of print].

[26] S.L. Green, R.A. Freiberg and A. Giaccia. p21$^{\text{Cip1}}$ *and* p27$^{\text{Kip1}}$ *regulate cell cycle reentry after hypoxic stress but are not necessary for hypoxia-induced arrest*. Mol. & Cell. Biol. **21** (2001), 1196–1206.

[27] H.P. Greenspan . *Models for the growth of a solid tumour by diffusion*. Stud. Appl. Math. 52 (1972) 317-340.

[28] H.P Greenspan. *On the growth and stability of cell cultures and solid tumours*. J. theor. Biol. 56(1976), 229-242.

[29] L. Griffiths, K. Binley, S. Iqball, O. Kan, P. Maxwell, P. Ratcliffe, C.E. Lewis, A. Harris, S. Kingsman and S. Naylor, *The macrophage - a novel system to deliver gene therapy to pathological hypoxia*, Gene Therapy, **7** (2000), 255-262.

[30] G. Griffon-Etienne, Y. Boucher, C. Brekken, H.D. Suit and R.K. Jain . *Taxane-induced apoptosis decompresses blood vessels and lowers interstitial fluid pressure in solid tumours: clinical implications*. Cancer Res. **59**(1999), 3776-3782.

[31] T.L. Jackson. *Intracellular accumulation and mechanism of action of doxorubicin in a spatio-temporal tumor model*. J. Theor. Biol. **220**(2003), 201-13.

[32] T.L. Jackson, S.R. Lubkin and J.D. Murray. *Theoretical analysis of conjugate localization in two-step cancer chemotherapy* J. Math. Biol. **39**(1999), 353-376.

[33] R.K. Jain. *Delivery of molecular and cellular medicine to solid tumours*. Adv. Drug Delivery Rev. **46** (2001), 149-168

[34] R.K. Jain. *Molecular regulation of vessel maturation*. Nature Med. **9** (2003), 685–693.

[35] R.K. Jain. *Normalization of tumour vasculature: an emerging concept in antiangiogenic therapy*, Science, **307** (2005), 58–62.

[36] J. Keener and J. Sneyd. *Mathematical physiology*. Springer-Verlag, New York, NY (USA). (1998).

[37] N.L. Komarova and V. Mirinov . *On the role of endothelial progenitor cells in tumour neovascularisation*. J. theor. Biol. **235**(2005), 338-349.

[38] H. Levine, S. Pamuk, B.D. Sleeman and M. Nilsen-Hamilton . *Mathematical modelling of capillary formation and development in tumour angiogenesis: penetration into the stroma*. Bull. Math. Biol. **63**(2001), 801-863.

[39] P.K. Maini, T. Alarcón, H.M. Byrne, M.R. Owen, J. Murphy. *Structural adaptation in normal and cancerous vasculature*. In *Math everywhere. A volume dedicated to Vincenzo Capasso's 60th birthday*. Ed. G. Aletti, M. Burger, A. Micheletti and D. Morale. To appear.

[40] N.V. Mantzaris, S. Webb, H.G. Othmer *Mathematical modelling of tumour-induced angiogenesis*. J. Math. Biol. **49** (2004), 111–187.

[41] R.J. Mayer, *Two steps forward in the treatment of colorectal cancer*, N. Engl. J. Med. **350** (2004), 2406–2408.

[42] S.R. McDougall, A.R.A. Anderson, M.A.J. Chaplain, *Mathematical modelling of dynamic adaptive tumour-induced angiogenesis: Clinical implications and therapeutic targeting strategies*. J. theor. Biol. In press.

[43] S. McDougall, A.R.A. Anderson and M.A.J. Chaplain . *Mathematical modelling of dynamic adaptive tumour-induced angiogenesis: clinical implications and therapeutic targeting strategies.* J. theor. Biol. (2006), (to appear)

[44] J. Moreira and A. Deutsch. *Cellular automaton models of tumor development: A critical review*, Adv. Complex Systems **5** (2002) 247–267.

[45] R.A. Morgan, M.E. Dudley, J.R. Wunderlich, M.S. Hughes, J.C. Yang, R.M. Sherry, R.E. Royal, S.L. Topalian, U.S. Kammula, N.P. Restifo, Z.Zheng, A.Nahvi, C.R. deVries, L.J. Rogers-Freezer, S.A. Mavroukakis, and S.A. Rosenberg, *Cancer regression in patients after transfer of genetically engineered lymphocytes*, Science, (2006), 1129003.

[46] H.G. Othmer and A. Stevens. *Aggregation, Blowup and Collapse: The ABC's of generalized taxis.* SIAM J. Applied Math. **57** (1997), 1044-1081.

[47] M.R. Owen, H.M. Byrne and C.E. Lewis . *Mathematical modelling of the use of macrophages as vehicles for drug delivery to hypoxic tumour sites.* J. theor. Biol. **226**(2004), 377-391.

[48] A.A. Patel, E.T.Gawlinski, S.K. Lemieux, R.A. Gatenby. *A cellular automaton model of early tumor growth and invasion: The effects of native tissue vascularity and increased anaerobic tumor metabolism.* J. theor. Biol. **213** (2001), 315–331.

[49] J. Philipp-Staheli, S.R. Payne and C.J. Kemp. *p27(Kip1): regulation and function of haploinsufficient tumour suppressor and its misregulation in cancer* Exp. Cell. Res. **264** (2001), 148–168.

[50] L. Preziosi . *Cancer modelling and simulation.* Chapman and Hall/CRC, (2003).

[51] A.R. Pries, T.W. Secomb, P. Gaehtgens. *Structural adaptation and stability of microvascular networks: theory and simulations.* Am. J. Physiol. (1998) **275**, H349–H360.

[52] A.R. Pries, B. Reglin, T.W. Secomb. *Structural adaptation of microvascular networks: functional response to adaptive responses.* Am. J. Physiol. (2001) **281**, H1015–H1025.

[53] V. Quaranta, A.M. Weaver, P.T. Cummings, A.R.A. Anderson . *Mathematical modeling of cancer: the future of prognosis and treatment.* Clin. Chim. Acta **357**(2005), 173-179.

[54] B. Ribba, K. Marron, Z. Agur, T. Alarcón, and P.K. Maini. *A mathematical model of Doxorubicin treatment efficacy on non-Hodgkin lymphoma: investigation of current protocol through theoretical modelling results.* Bull. Math. Biol. **67**, 79-99 (2005).

[55] N. Resnick, H. Yahav, A. Shay-Salit, M. Shushy, S. Schubert, L.C.M. Zilberman, E. Wofovitz. *Fluid shear stress and the vascular endothelium: for better and for worse.* Progress Biophys. Mol. Biol. (2003) **81**, 177–199.

[56] T. Roose, S.J. Chapman and P.K. Maini . *Mathematical models of avascular tumour growth: a review.* SIAM Review (2006),(in press).

[57] J.A. Royds, S.K. Dower, E.E. Qwarstrom and C.E. Lewis. *Response of tumour cells to hypoxia: role of p53 and NF$\kappa\beta$.* J. Clin. Path.: Mol. Pathol. **51** (1998), 55-61.

[58] K. Smallbone, D.J. Gavaghan, R.A. Gatenby and P.K. Maini . *The role of acidity in solid tumour growth and invasion.* J. Theor. Biol. **235**(2005), 476-484.

[59] K. Smallbone, R.A. Gatenby, R.J. Gillies, P.K. Maini and D.J. Gavagan. *Metabolic changes during carcinogenesis: Potential impact on invasiveness*, (2006), (submitted).

[60] R.H. Smallwood, W.M.L. Holcombe and D.C. Walker . *Development and validation of computational models of cellular interaction.* J. Mol. Hist. **35**(2004), 659-665.

[61] A. Stephanou, S.R. McDougall, A.R.A. Anderson and M.A.J. Chaplain . *Mathematical Modelling of Flow in 2D and 3D Vascular Networks: Applications to Anti-angiogenic and Chemotherapeutic Drug Strategies*, Math. Comp. Model., **41** (2005), 1137-1156.

[62] A. Stéphanou, S.R. McDougall, A.R.A. Anderson, M.A.J. Chaplain. *Mathematical modelling of the influence of blood rheological properties upon adaptive tumour-induced angiogenesis*, Math. Comp. Model., (2006), **44**:96–123.

[63] E.L. Stott, N.F. Britton, J.A. Glazier and M. Zajac. *Stochastic simulation of benign avascular tumour growth using the Potts model.* Math. Comp. Mod. **30** (1999), 183-198.

[64] K.R. Swanson, E.C. Alvord and J.D. Murray. *A quantitative model for differential motility of gliomas in grey and white matter.* Cell. Prolif. **33** (2000), 317-329.

[65] K.R. Swanson, E.C. Alvord and J.D. Murray . *Quantifying efficacy of chemotherapy of brain tumors with homogeneous and heterogeneous drug delivery.* Acta Biotheoretica 50 (2002), 223-237.

[66] K.R. Swanson, C. Bridge, J.D. Murray and E.C. Alvord, E.C.. *Virtual and real brain tumors: using mathematical modeling to quantify glioma growth and invasion.* J. Neur. Sci. 216 (2003), 1-10.

[67] B.A. Teicher, *A systems approach to cancer therapy*, Cancer Metastasis Rev., **15** (1996), 247–272.

[68] R.T. Tong, Y. Boucher, S.V. Kozin, F. Winkler, D.J. Kicklin, R.K. Jain. *Vascular normalisation by VEGFR2 blockade induces a pressure gradient accross the vasculature and improves drug penetration tumours.* Cancer Res. **64** (2004), 3731–3736.

[69] J.J. Tyson and B. Novak. *Regulation of the eukariotic cell-cycle: molecular anatagonism, hysteresis, and irreversible transitions.* J. Theor. Biol. **210** (2001), 249–263.

[70] F. Winkler, S.V. Kozin, R.T. Tong, S-S. Chae, M.F. Booth, I. Garkavtsev, L. Xu, D.J. Hicklin, D. Fukumura, E. di Tomaso, L.L. Munn, R.K. Jain. *Kinetics of vascular normalisation by VEGFR2 blockade governs brain tumour response to radiation: Role of oxygenation, angiopoietin-1 and matrix metalloproteinases.* Cancer Cell, **6** (2004), 553–563.

[71] G.D. Yancopoulos, S. Davis, N.W. Gale, J.S. Rudge, S.J. Wiegand, J. Holash. *Vascular-specific growth factors and blood vessel formation.* Nature. **407** (2000), 242–248.